Preprint typeset using LaTeX style emulateapj v. 03/07/07

arXiv:0902.2378v1 [astro-ph.GA] 13 Feb 2009

CHEMICAL ABUNDANCE PATTERNS IN THE INNER GALAXY: THE SCUTUM RED SUPERGIANT CLUSTERS

Ben Davies[1], Livia Origlia[2], Rolf-Peter Kudritzki[3], Don F. Figer[1], R. Michael Rich[4], Francisco Najarro[5], Ignacio Negueruela[6], J. Simon Clark[7]

[1]Chester F. Carlson Center for Imaging Science, Rochester Institute of Technology, 54 Lomb Memorial Drive, Rochester NY, 14623, USA
[2]INAF - Osservatorio Astronomico di Bologna, via Ranzani 1, 40127 Bologna, Italy
[3]Institute for Astronomy, University of Hawaii, 2680 Woodlawn Drive, Honolulu, HI, 96822, USA
[4]Department of Physics and Astronomy, UCLA, 430 Portola Plaza, Box 951547, Los Angeles, CA 90095-1547, USA
[5]Instituto de Estructura de la Materia, Consejo Superior de Investigaciones Cientificas, Calle Serrano 121, 28006 Madrid, Spain.
[6]Departamento. de Física, Ingeniería de Sistemas y Teoría de la Señal, Universidad de Alicante, Apdo. 99, E03080 Alicante, Spain and
[7]Department of Physics & Astronomy, The Open University, Walton Hall, Milton Keynes, MK7 6AA, UK

ABSTRACT

The location of the Scutum Red-Supergiant (RSG) clusters at the end of the Galactic Bar makes them an excellent probe of the Galaxy's secular evolution; while the clusters themselves are ideal testbeds in which to study the predictions of stellar evolutionary theory. To this end, we present a study of the RSGs' surface abundances using a combination of high-resolution Keck/NIRSPEC H-band spectroscopy and spectral synthesis analysis. We provide abundance measurements for elements C, O, Si, Mg, Ti, and Fe. We find that the surface abundances of the stars studied are consistent with CNO burning and deep, rotationally enhanced mixing. The average α/Fe ratios of the clusters are solar, consistent with a thin-disk population. However, we find significantly sub-solar Fe/H ratios for each cluster, a result which strongly contradicts a simple extrapolation of the Galactic metallicity gradient to lower Galacto-centric distances. We suggest that a simple one-dimensional parameterization of the Galaxy's abundance patterns is insufficient at low Galactocentric distances, as large azimuthal variations may be present. Indeed, we show that the abundances of O, Si and Mg are consistent with independent measurements of objects in similar locations in the Galaxy. In combining our results with other data in the literature, we present evidence for large-scale (∼kpc) azimuthal variations in abundances at Galacto-centric distances of 3-5 kpc. While we cannot rule-out that this observed behaviour is due to systematic offsets between different measurement techniques, we do find evidence for similar behaviour in a study of the barred-spiral galaxy NGC 4736 which uses homogeneous methodology. We suggest that these azimuthal abundance variations could result from the intense but patchy star formation driven by the potential of the central bar.

Subject headings: open clusters & associations, supergiants, stars:evolution, stars:late-type, Galaxy: abundances, Galaxy: evolution, Galaxy: disk

1. INTRODUCTION

Massive young clusters are powerful natural laboratories with which to study many different aspects of astrophysics. They contain large numbers of coeval stars with similar initial chemical compositions. Their youth and large initial masses mean that they contain many massive stars, and hence are intrinsically very bright objects. Thus, such clusters can be used to make critical tests of stellar evolution, while they also trace recent star-forming history and local abundance patterns.

Two such clusters exist in the constellation of Scutum, at distances of ∼6 kpc. They are among the most massive young clusters in the Galaxy, with initial masses in excess of $10^4 M_\odot$. Their ages are tuned in such a way that their most massive remaining stars are in the Red Supergiant (RSG) phase, and together these clusters contain ∼20% of all known RSGs in the Galaxy – cluster 1 (hereafter RSGC1) contains 14 RSGs, while cluster 2 (RSGC2) contains 26 (Figer et al. 2006; Davies et al. 2007, 2008a, hereafter F06, D07, D08).

The clusters are located in the Galactic Plane, and have high visual extinctions ($A_V \approx 25$ and 16 for RSGC1 and RSGC2 respectively). However, the fluxes of the RSGs peak at ∼1μm, making them extremely bright in the near-IR where the extinction is reduced. Hence, the RSGs themselves make excellent tools with which to probe the global properties of their host clusters.

The clusters' distances from Earth and Galactic longitude place them at Galacto-centric distances of ∼3.5 kpc, and at an azimuthal angle $\phi_{GC} = 45 \pm 10°$ relative to the Sun-Galactic Centre axis. This places them at the tip of the Galactic Bar as described by Benjamin et al. (2005), which has half-length 4.5kpc and $\phi_{GC} = 44 \pm 10°$. This raises the intriguing possibility that the RSG clusters were formed in a region-wide starburst event, triggered by the interaction between the Bar and the disk. Aside from the two clusters, there is certainly plenty of other evidence for recent star-forming activity along this line-of-sight: D07 found several other red stars in the field of RSGC2, which while not belonging to the cluster, were likely to be supergiants and hence massive stars. This is consistent with the large number of RSGs found at the base of the Scutum spiral arm found by López-Corredoira et al. (1999). Also noted in D07 were other objects indicative of recent star-forming activity, such as the candidate supernova remnant IRAS 18369-0557 and the candidate massive evolved star IRAS 18367-0556; while Gotthelf & Halpern (2008) have identified the TeV gamma-ray source HESS J1837-069 with possibly two young pulsar wind-nebulae.

In this paper we assess the chemical abundances of the two clusters, using high-resolution H-band spectroscopy of a sample of RSGs in each cluster, in combination with LTE model atmospheres. Our method allows us to derive abundances for C, Fe, and the α-elements O, Ca, Si, Mg, and Ti. We use these chemical abundances to address two distinct topics.

Firstly, we use the relative surface abundances to test the predictions of stellar evolutionary models. In massive stars, the primary route of H fusion is via the CNO-cycle. Due to the relative reaction rates involved in this cycle, a depletion of carbon occurs at the expense of nitrogen. As stars enter the RSG phase, their deep convective layers are expected to bring the products of nuclear burning to the surface. Thus, the relative C abundances in the atmospheres of the RSGs allow us to make critical tests of the latest stellar evolution codes, such as those which include rotation (e.g. Meynet & Maeder 2000) and the interaction with binary companions (e.g. Eldridge et al. 2008).

Secondly, we will use the relative abundances of Fe and several α-elements in the RSG clusters, in combination with the clusters' coincidence with the Galactic Bar, to investigate the star-formation history of the Galaxy. The dominant source of α enrichment in the Interstellar Medium (ISM) is through type-II supernovae (SNe), i.e. the core-collapse of massive stars. On the other hand, Fe-peak elements are produced in type-Ia SNe – thermonuclear explosions of low mass stars which reach the Chandrasekhar limit through accretion from a companion. Hence, α-elements are enriched on short ($\sim$Myr) timescales, while Fe-peak abundances are increased over much longer timescales ($\sim$Gyr).

In our Galaxy, we see variations in the [α/Fe] ratio: in the central Galactic Bulge, at Galacto-centric distances of $R_{\rm GC} \lesssim 2\,$kpc, the [α/Fe] ratio is found to be super-solar from analyses of Red Giants (Rich & Origlia 2005; Cunha & Smith 2006; Fulbright et al. 2006, 2007; Lecureur et al. 2007). In the 'thin' Galactic disk at $R_{\rm GC} \gtrsim 5\,$kpc and scale height $|h| \lesssim$100pc, the ratio α/Fe is found to be closer to solar (Bensby et al. 2004; Luck et al. 2006, and references therein). In addition, the relative abundances in the thin disk are a function of $R_{\rm GC}$: there is evidence to suggest heavy elemental abundance levels increase at lower Galacto-centric distances, while the ratio [α/Fe] increases in the outer disk (e.g Luck et al. 2006; Yong et al. 2006).

These abundance patterns are commonly explained as being due to the distinct star-formation histories of the different Galactic environments. The Bulge was formed rapidly several Gyrs ago, in a starburst event which was too brief for the chemical evolution to be affected by Type-Ia SNe. In the disk, star-formation has continued over the lifetime of the Galaxy, allowing Type-Ia SNe to contribute to the chemical enrichment of the ISM.

In the inner disk ($R_{\rm GC} \lesssim 5\,$kpc), the abundance patterns are thought to be strongly influenced by the Bar. External galaxies with bars are found to have significantly flatter abundance gradients than those without (Martin & Roy 1994; Zaritsky et al. 1994). This is explained as being due to radial motions induced by the bar potential (Friedli et al. 1994; Friedli & Benz 1995). In addition, pile-up of material at the bar's resonances can create star-forming hot-spots which result in localised chemical enrichment. The RSG clusters themselves are evidence of such a localised starburst in the inner regions of our own Galaxy, and have Galactocentric distances similar to co-rotation ($\sim$3.5kpc) and the Outer Lindblad Resonance ($\sim$5kpc).

In this paper, we will explore the chemical abundances of the inner disk from analyses of the RSGs in the two Scutum clusters. By comparing to other abundance measurements in the inner disk, we will probe the star forming history in a region which is pivotal in the Galaxy's secular evolution.

The paper is organized as follows: in Sect. 2 we describe our observations, data-reduction steps and analysis techniques; in Sect. 3 we present our results and discuss the abundance patterns of the two clusters. We make quantitative comparisons of these results with stellar evolutionary models in Sect. 4, while in Sect. 5 we discuss the abundances of the two clusters in the context of those of the inner Galaxy. We conclude in Sect. 6.

2. OBSERVATIONS, DATA REDUCTION & ANALYSIS

Observations were taken during the night of 13th Aug 2006 using NIRSPEC, the cross-dispersed echelle spectrograph mounted on Keck-II (McLean et al. 1995). The instrument was used in high-resolution mode with the $0.576'' \times 12''$ slit and the NIRSPEC-5 filter. We used a dispersion angle of 63.0° and a cross-dispersion angle of 36.72°. This achieved a spectral resolution of $\sim$17,000 at select regions within the wavelength range of 1.5-1.7μm.

We used integration times of 20s, and observed each star twice at different positions nodded along the slit. We observed all 14 RSGs in RSGC1, and 12 RSGs from RSGC2. The identifications of the specific stars observed, taken from Figer et al. (2006) and Davies et al. (2007), can be found in Table 3. In addition to the cluster stars, we also observed HD 171305 (spectral type B0 V) as a telluric standard. Flat-field images were taken with a continuum lamp, while for wavelength calibration we observed Ar, Ne, Xe and Kr arc lamps, to provide a large number of template lines in the narrow wavelength range of each spectral order.

Removal of sky emission, dark current and bias offset was done by subtracting nod-pairs, and images were flat-fielded with the continuum-lamp exposures. The spectral traces produced by NIRSPEC are warped in both the spatial and dispersion directions, so before extracting the spectra from the reduced science frames each two-dimensional order was rectified onto a linear grid. The spatial warping was characterized by the spectral traces of the two stellar traces in a nod pair. The distortion in the dispersion direction was fitted using the arc- and etalon-lines. For technical details of the rectification process, see Figer et al. (2003).

As we know the wavelengths of the arc-lines, rectification also wavelength calibrates the data. By rectifying the arc frames and measuring the residuals of the arc-line wavelengths, we found the wavelength solution to be accurate to $\pm 4\,$km s^{-1} across all orders.

Spectra were extracted by summing each channel in the rectified orders within $\pm 5\sigma$ of the centre of each spectrum. Cosmic-ray hits and bad pixels were identified by comparing the two nod spectra of each star, and were replaced by the median value of the closest 4 pixels.

We removed the H and He I absorption features of the telluric standard via linear interpolation either side of the line. The atmospheric absorption features in the science frames were then removed by dividing through by the telluric standard. Finally, the spectra were normalised by dividing through by the median continuum value. From featureless continuum regions in the final spectra, we estimate the signal-to-noise to be better than 100 for all spectra.

2.1. *Data analysis*

In order to obtain chemical abundances from the spectra, we have developed a technique of generating synthetic spectra from cool star model atmospheres, and adjusting the input relative abundances to match the equivalent widths of certain diagnostic lines. The code used is that presented in Origlia et al. (1993), which was updated in Origlia et al. (2002, 2003). The code has been used successfully to obtain abundances of Bulge giants (e.g. Rich & Origlia 2005), young clusters dominated by RSGs (e.g. Larsen et al. 2008), and most recently to study the chemical abundandes of RSGs in the Galactic Centre (Davies et al. 2008b).

The code and methodology is explained in detail in the papers listed above. Briefly, the code uses the LTE approximation and model atmospheres from the grid of Johnson et al. (1980) which incorporate the effect of molecular blanketing. Thousands of near-IR molecular ro-vibrational and atomic transitions are included. Initial estimates of the stars' luminosities, temperatures and surface gravities were estimated based on the results of D07 and D08, while the microturbulent velocity ξ is estimated from the OH and CO lines. We were able to produce satisfactory fits to the data without the inclusion of macroturbulence. This is to be expected for observations of RSGs with initial masses $\sim$10-20$M_{\odot}$, whose macroturbulent velocities are often found to be comparable to the spectral resolution of our observations (see also Davies et al. 2008b).

Abundance estimates are obtained by adjusting relative abundances in the model atmospheres, computing the synthetic spectra, and minimizing the residuals between the observed and synthetic spectra in the equivalent widths of certain diagnostic lines. We concentrate on fitting those lines which are relatively unblended and for which reliable atomic/molecular data exist. The ro-vibrational lines of OH and CO are used to determine oxygen and carbon abundances, while abundances of other metals are derived from the atomic lines of Fe I, Si I, Mg I, Ca I, and Ti I. While the molecule CN is included in the analysis, severe blending of the lines at the observed spectral resolution prevents an accurate determination of the N abundance. We do however find results that are consistent with CNO equilibrium, that is with N being enhanced by the same level that C is depleted. For compilations of atomic/molecular data we use the Kurucz database[1], Biemont & Grevesse (1973), Huber & Herzberg (1979), Sneden & Lambert (1982), and Meléndez & Barbuy (1999).

For each best-fitting model, we estimate the uncertainties and solution-robustness by generating a further four models with abundances $\pm$0.1dex and $\pm$0.2dex. In addition, test models are generated in which the stellar parameters are varied and the abundances re-tuned, to assess the degeneracy of the model solutions. In studying the residuals between the test-models and the observed spectra, we find that solutions of similar statistical significance are found with $\Delta T_{\rm eff} \pm 200\,$K, $\Delta \log g = \pm 0.3$, and $\Delta\xi = \mp 0.5\,$km s^{-1}, which we take to be the uncertainties on the stellar parameters. We find that the measured abundances are stable across the test models to within 0.1-0.2dex, while we found that gravities $\log g = 0.0 \pm 0.3$ and microturbulence $\xi = 3 \pm 0.5\,$km s^{-1} produced satisfactory fits for all stars modelled. The quoted errors include the uncertainty on the continuum placement when measuring the line equivalent widths, which can be problematic in H-band spectra of cool stars due to the number of spectral features. As a further cross-check on our results, we re-ran the spectral sysnthesis using the CN line-list provided by B. Gustafsson (priv. comm.), finding negligible differences in derived abundances (see Fig. 1).

Finally, as further validation of our method we note that in our recent study of two RSGs in the Galactic Centre, we found that our results were consistent with those of complimentary studies of the same objects to within our quoted uncertainties (Davies et al. 2008b), while in a study of Arcturus we found abundances consistent with previous measurements (Rich & Origlia 2005).

3. RESULTS

Selected regions of the H-band spectra of one star in each cluster are shown in Fig. 1. Each show a dense absorption line spectrum, dominated by neutral lines of Fe, several α elements (Si, Ca, Mg, Ti), as well as molecular bands of OH and CO. Below, we describe the abundance patterns of the elements studied. As reference, we use the solar abundances of Asplund et al. (2005).

The elemental abundances we derive for each star are listed in full in Appendix A. To within the uncertainties, the elemental abundances for each star studied in each cluster are consistent. In Table 1, we show the average abundance for each element in each cluster. Here, it can be seen that the average abundances in the two clusters are similar to within the errors. This evidence, together with the proximity of the clusters to one another ($d_{sep} = 0.8^{+1.6}_{-0.7}$kpc, D08) and their similar ages (D07, D08), suggests that the two clusters formed out of the same giant molecular cloud.

We find that, in general, both clusters are slightly metal-poor with respect to the solar value. The Fe content averaged over the two clusters is [Fe/H] $= -0.15 \pm 0.07$. The α-elements (Ca, O, Mg, Si, Ti) also show abundances which are $\sim$0.1-0.2dex below the solar level. These values do not take into account self-depletion of H at the surfaces of the stars: in Davies et al. (2008b) we show, with the aid of evolutionary models, that the atmospheres of RSGs can be depleted in H by up to 0.1dex, as the deep convective layers draw the nuclear-processed material to the surface. Therefore, we conclude that the *initial* [Fe/H] and [α/H] ratios of the two clusters were $\approx$0.2-0.3dex below solar.

The ratio of the α-elements to Fe, which is a powerful probe of star-formation history (see Sect. 1), is consistent with solar for each of Si, Mg, Ca and Ti. We find [O/Fe] $= +0.09 \pm 0.11$ using the Asplund et al. (2005) so-

[1] http://cfa-www.harvard.edu/amdata/ampdata/kurucz23/sekur.html

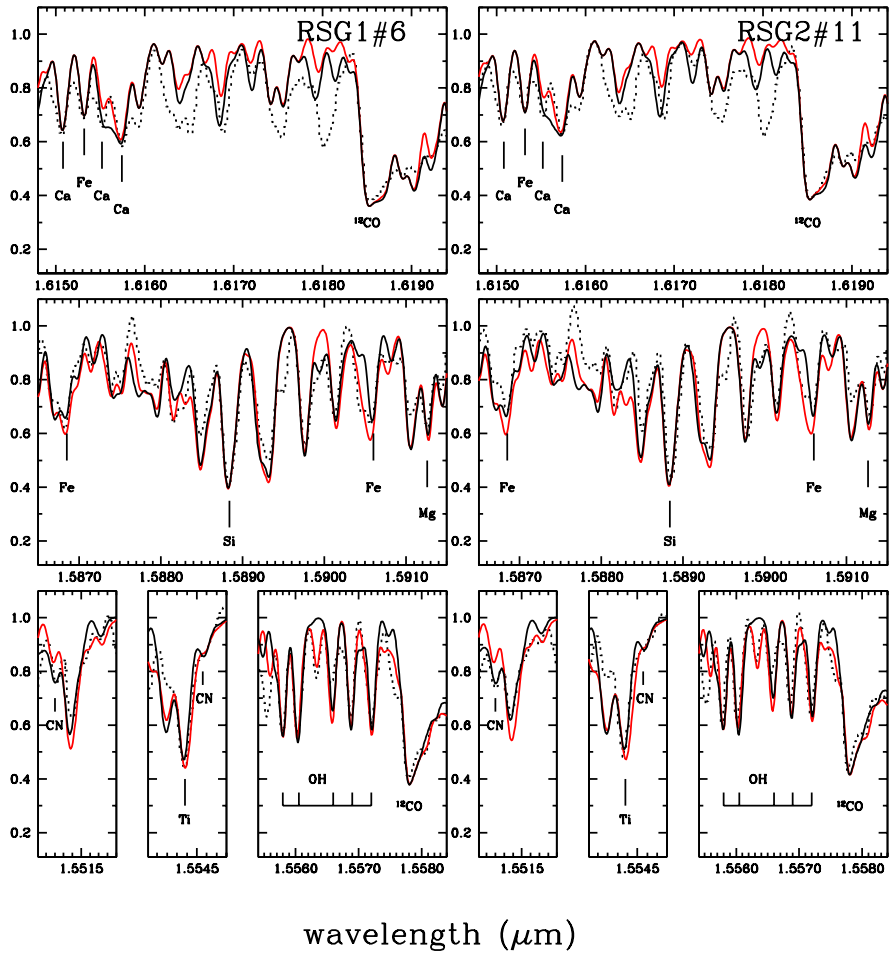

Fig. 1.—: Examples of the H-band spectra of one star in each cluster, showing select regions and the identified lines. Observations are shown as dotted lines, our best-fit synthetic spectra are shown as solid black lines. In addition, we also plot the computed best-fit spectrum using the Uppsala CN line-list (B. Gustavsson, priv. comm. – solid red lines), with negligible differences in the strengths of the diagnostic lines.

TABLE 1:
Average elemental abundances of the two clusters, where $A(X) = \log(X/H) + 12$. Columns show (1) the elements studied; (2) the mean solar abundances, taken from Asplund et al. (2005); (3) & (4) the average abundances for RSGC1 and RSGC2 respectively; and (5) the ratio of each element's average abundance from the two clusters compared to Fe, normalized to the solar value. The uncertainties in the average cluster abundances are taken as the rms standard deviation in each value.

Element X	$A(X)_{\odot}$	$A(X)_{\rm RSGC1}$	$A(X)_{\rm RSGC2}$	$[X/{\rm Fe}]_{\rm RSGC1}$	$[X/{\rm Fe}]_{\rm RSGC2}$
Fe	7.45	7.33	7.28	–	–
–	± 0.05	± 0.05	± 0.03	–	–
O	8.66	8.61	8.59	0.08	0.10
–	± 0.05	± 0.07	± 0.05	± 0.11	± 0.09
Si	7.51	7.30	7.36	-0.08	0.02
–	± 0.04	± 0.08	± 0.08	± 0.12	± 0.11
Mg	7.53	7.41	7.36	0.00	-0.00
–	± 0.09	± 0.13	± 0.09	± 0.17	± 0.14
Ca	6.31	6.20	6.18	0.02	0.04
–	± 0.04	± 0.05	± 0.04	± 0.10	± 0.08
Ti	4.90	4.92	4.92	0.14	0.19
–	± 0.06	± 0.10	± 0.06	± 0.14	± 0.08
C	8.39	7.95	7.89	-0.32	-0.33
–	± 0.05	± 0.07	± 0.06	± 0.11	± 0.10

lar abundances. When the Grevesse & Sauval (1998) solar values are used, we find [O/Fe] = -0.03 ± 0.11. Given the recent fluctuations in the derived solar O abundance, at this time we conclude for now that the O/Fe ratio in the clusters is consistent with solar.

The levels of carbon in the stars' atmospheres appear to be significantly depleted, consistent with their evolved status. This result is expanded upon in detail in Sect. 4.

4. COMPARISON WITH STELLAR EVOLUTIONARY MODELS

The results presented in Sect. 3 allow us to test various predictions of stellar evolutionary models. As stars enter the RSG phase, the products of CNO burning are expected to be seen at the surface, specifically the enrichment of N at the expense of C. From the values in Table 3, it can be seen that all stars in both clusters show evidence of C depletion. In Fig. 2 we investigate quantitatively the predictions for surface C abundances as a function of evolutionary state.

Throughout our analysis, we consider the C fraction in relation to the Fe abundance. In evolutionary models, the relative abundance of an element X with respect to hydrogen X/H depends on two input parameters: the relative abundances of the heavy elements, and the ratio of the heavy element abundances to H (i.e. the metallicity, Z). However, the ratio X/Fe depends only on the relative abundances of the heavy elements. Thus, by comparing C as a function of Fe, we reduce the model-dependency of our analysis. As the relative abundances of the heavier elements in the stars studied here appear to be consistent with solar (see Table 1), we use models with solar-scaled heavy element abundances.

4.1. *Non-rotating models vs rotating models*

In Fig. 2 (*left*) we plot the C/Fe fraction as a function of luminosity for the stars observed. The stellar luminosities are taken from D07 and D08. Overplotted are mass tracks at initial masses of $12M_{\odot}$, $15M_{\odot}$ and $20M_{\odot}$ from the non-rotating Geneva models. For reference, the initial masses of the RSGs in each cluster (derived from the rotating Geneva models) are $18M_{\odot}$ for RSGC1 and $14M_{\odot}$ for RSGC2 (D08). As we find a sub-solar iron content for the stars in each cluster, we plot tracks using both solar metallicity (Z=0.02 Schaller et al. 1992) and Z=0.008 (Schaerer et al. 1993). The iron content we derive for the RSG clusters indicates a metallicity somewhere between these two values. In the right-hand panel of Fig. 2, we plot the same quantities in comparison to the Geneva models which include rotation, at $Z = 0.02$ and $Z = 0.004$ (Meynet & Maeder 2000; Maeder & Meynet 2001, respectively)[2]

When comparing our derived C abundances with those predicted by the Geneva evolutionary models, it is important to first note that these models use the relative heavy elemental abundances of Grevesse & Sauval (1998). In the 3-D solar model of Asplund et al. (2005) the fractional abundances of C and Fe have been revised slightly. For this analysis we assume that this small change in relative metal abundances would have no major impact on the output of the Geneva evolutionary code other than to cause a linear displacement in abundance-space. We have shifted each mass track by 0.105dex – the magnitude of the revision in the Solar [C/Fe] fraction. We indicate the magnitude of this displacement with an arrow in the upper-right of each of the panels in Fig. 2.

In general, the non-rotating models do not quite reproduce the observed level of C depletion in the RSGs of the two Scutum clusters, even when the updated solar [C/Fe] is taken into account (Fig. 2, *left*). There seems to be much better agreement between the data and the rotating models, which are more heavily depleted than the non-rotating models due to rotationally-enhanced internal mixing. Sub-Solar metallicity models suffer a slightly greater level of C depletion, due to decreased mass-loss on the main sequence which inhibits the loss of angular momentum and increases the level of internal mixing. This can be seen in the right-hand panel of Fig. 2, where the low-Z mass-tracks have systematically lower C/Fe ratios. While we are unable to discern between the Solar and sub-Solar mass-tracks, we can say that the rotating models provide a much better fit to the [C/Fe] levels, while it has already been shown that these models do a better job of reproducing the luminosity distributions of the two clusters (D08).

4.2. *Binary models*

To assess the impact of binarity on surface abundances we refer to the Cambridge binary star evolution code presented in Eldridge et al. (2008). The code includes the effect of Roche Lobe Overflow and Common-Envelope Evolution, processes which are particularly important when the primary star evolves to the RSG phase due to the expanded atmosphere.

Briefly, the evolution to the RSG phase of a massive star can result in the star filling its Roche Lobe and transferring matter to the companion star. This reveals the lower layers of the primary's atmosphere in which the effects of CNO burning are more evident. However, mass-transfer of the primary's envelope onto the secondary also restricts the primary's redward evolution, resulting in drastically shortened RSG lifetimes. Eldridge et al. (2008) showed that, for a sample of binary systems with broad distributions of separations and mass-ratios, the *mean* RSG lifetime averaged across the sample was reduced by a factor of $\sim$3. However, for low-separation binary systems the RSG lifetime-reduction is clearly much more severe. Therefore, the chances of observing a RSG in a close binary are extremely small, given the brevity of the phase in single stars ($t_{\rm RSG}$ $\sim$1Myr for a single star in the Eldridge et al. models).

While binary models are able to increase the level of C depletion, the drastically reduced RSG lifetimes lead us to conclude that close binary interaction cannot have played a significant role in the evolution of the RSGs in the two clusters. This is not to say that binarity is not prevalent in the clusters, more that the RSGs in the two clusters that we see today are unlikely to have evolved in a close binary system. This has two important implications, which we now discuss.

Firstly, in F06, D07 and D08, the masses of the clusters were estimated by counting the numbers of RSGs, comparing to population synthesis models created using single star evolutionary codes, and extrapolating over the rest of the Initial Mass Function. If the clusters have

[2] Geneva rotating models at Z=0.008 are unavailable at the time of writing.

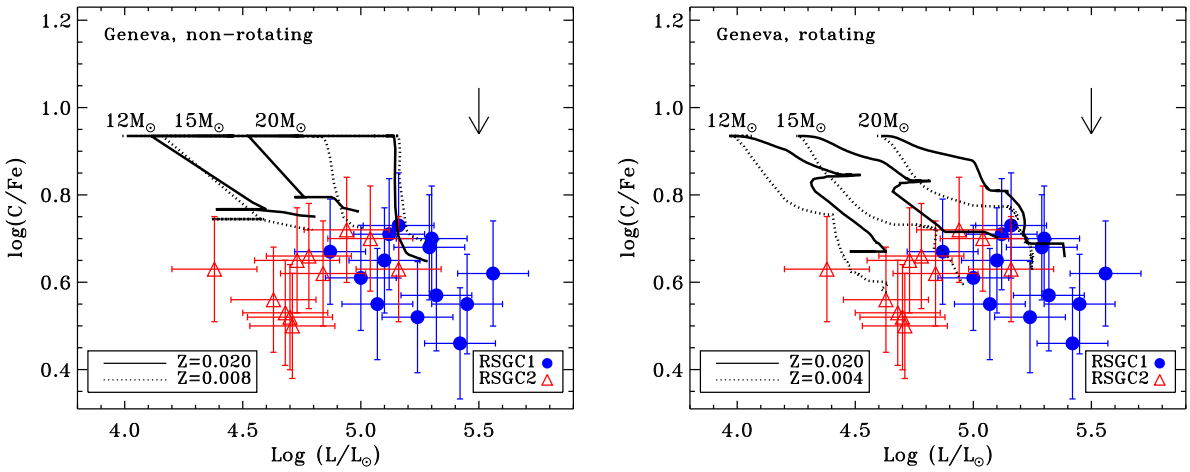

Fig. 2.—: Carbon fraction as a function of stellar luminosity. Overplotted are mass-tracks from the Geneva non-rotating (*left*) and rotating (*right*) isochrones at solar and sub-solar metallicities (see text for references). Note that the sub-solar metallicities are different in each panel. The mass-tracks have been shifted downwards to reflect the recent revision in the Solar [C/Fe] – the arrow in the top-right of each panel indicates the magnitude of this change (see text for details).

high binary fractions, then a significant number of cluster members which had the same initial masses of the RSGs we see now will have skipped the RSG phase. The not-unreasonable parameters for a binary distribution used by Eldridge et al. suggest a reduction in the number of RSGs by a factor of ∼3 compared with single-star models. Therefore, the total cluster masses may have been underestimed by a similar factor, implying initial masses in excess of $10^5 M_\odot$, which would make them the most massive young clusters in the Galaxy.

Secondly, the mere fact that we are looking at RSGs in these clusters suggests that we are dealing with stars which have in effect evolved in isolation. That is, it is reasonably safe to assume that the stars are *single*. This is an extremely important consideration if we are to use the stars to measure the velocity dispersion of the clusters, and hence determine their virial masses. Contamination by the high orbital velocities in close massive binaries would lead to a significant systematic overestimate of a sample's velocity dispersion, and hence of the virial mass. On the one hand, this should serve as a note of caution when interpreting the velocity dispersions in young massive clusters when measured from blue stars, particularly as the massive binary fraction of Westerlund 1 has recently been inferred to be very high (Clark et al. 2008). On the other hand, this would also seem to suggest that RSG spectral features provide the most reliable measurement of cluster velocity dispersions (see e.g. Mengel et al. 2008).

5. THE RSG CLUSTERS AND THE STAR-FORMATION HISTORY OF THE GALAXY

In this section, we compare the relative abundances derived for the RSG clusters with the standard indicators of star-formation history, namely the ratios [Fe/H] and [α/Fe]. In broad terms, the primary source of α-element enrichment in the Galaxy is through Type-II supernovae (SNe), that is the core-collapse of stars with masses greater than $\sim 8 M_\odot$. On the other hand, the main source of Fe enrichment is SNe Ia – thermonuclear explosions of low mass stars which reach the Chandrasekhar limit through accretion from a companion. Hence, as Fe- and α-enrichment occurs on vastly different timescales, star-formation histories can be probed through comparisons of the α and Fe abundances

5.1. *The abundance patterns of the Galaxy*

In the Galactic 'thin' disk, with Galacto-centric distances $R_{GC} \gtrsim$4kpc and scale height $|h| \lesssim$ 100pc, it has been found from abundance analysis of Cepheids and late-type dwarfs that the ratio [α/Fe] is approximately solar (Bensby et al. 2004; Luck et al. 2006, and references therein). Meanwhile, in the 'thick' disk ($|h| \gtrsim$ 100pc), halo and bulge, [α/Fe] is found to be super-solar from analyses of Red Giants (Rich & Origlia 2005; Cunha & Smith 2006; Fulbright et al. 2006, 2007; Lecureur et al. 2007; Meléndez et al. 2008).

In addition, many authors have found evidence for a trend of increasing chemical abundances with decreasing R_{GC}, the so-called Galactic metallicity gradient. Analyses of B dwarfs (Rolleston et al. 2000; Smartt et al. 2001), Cepheids (Luck et al. 2006), UC-HII regions (e.g. Afflerbach et al. 1997), and Planetary Nebulae (e.g. Maciel & Quireza 1999) have all found evidence for increasing metal abundances, both of Fe and α-elements, at lower R_{GC}. Further, the results of Andrievsky and collaborators (summarised in Luck et al. 2006), who studied the abundances of both Fe and the α-element Ca in Cepheids, showed that [Ca/Fe] was solar and roughly constant throughout the thin disk out to $R_{\rm GC} \approx$ 8kpc, with tentative evidence for an increase in [Ca/Fe] in the outer Galaxy.

These abundance patterns are thought to be a result of the Galaxy's evolution and star-formation history: the bulge and halo formed very quickly (∼0.1-0.5Gyr, Ballero et al. 2007), during which time the chemical evolution was dominated by SNe II. After this time, star formation ceased and the α-heavy abundances were frozen-in. However, in the Galactic disk star-formation continued at some rate which was a function of R_{GC}. Eventually the enrichment of the Fe abundance by SNe Ia brought the α/Fe ratio to below that of the halo and bulge.

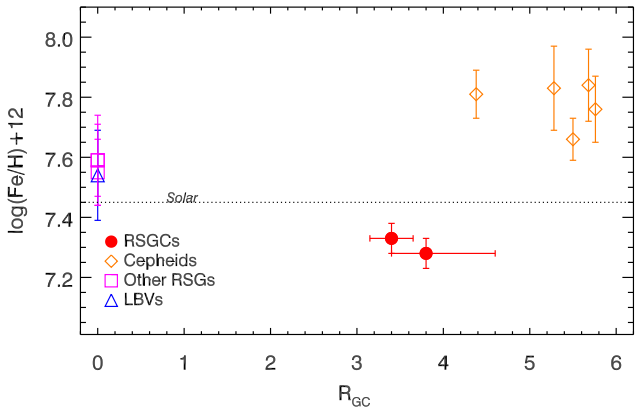

Fig. 3.—: The trend of Fe/H abundance in the inner 6kpc of the Galaxy. The dotted line in each panel indicates the relevant solar value from Asplund et al. (2005). The references for the literature data are given in Table 2.

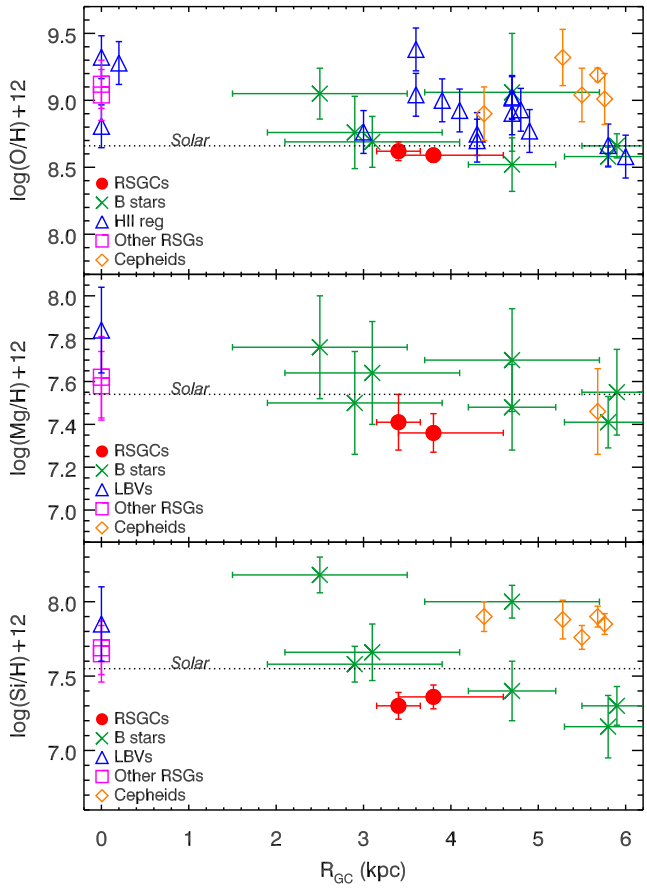

Fig. 4.—: Same as Fig. 3 but for oxygen (top panel), magnesium (middle panel) and silicon (bottom panel).

5.2. *Comparison between Galactic and RSGC abundances*

5.2.1. *Iron*

As stated in Sect. 3, we find that the average Fe/H abundance ratios for the two clusters are 0.1-0.2dex below solar. This is neglecting the effects of self-depletion in the atmopsheres in RSGs, which we estimate to be a further $\sim -0.05 - 0.1$dex for stars with initial masses of 14-18$M_{\odot}$ (see Fig. 2 of Davies et al. 2008b).

TABLE 2:
References for the data shown in Figures 3 - 6.

Object	References
B stars	Smartt et al. (2001); Daflon & Cunha (2004)
HII regions	Afflerbach et al. (1997)
Other RSGs	Davies et al. (2008b); Cunha et al. (2007)
LBVs	Najarro et al. (2008)
Cepheids	Andrievsky et al. (2002)

In Fig. 3 we compare the Fe/H ratios of the clusters with other Fe/H measurements in the inner Galaxy. In analysis of the atmospheres of Cepheids, Andrievsky et al. (2002); Luck et al. (2006) find that the Fe/H ratio increases towards the Galactic Centre (GC) at a rate of -0.06dex kpc^{-1}, reaching $\approx$+0.2dex above solar at $R_{\rm GC} \lesssim$ 6kpc. In the GC, recent studies suggest that the Fe abundance is roughly solar (Najarro et al. 2008; Davies et al. 2008b, e.g.). We note that Cunha et al. (2007) found slightly super-solar Fe levels from studies of RSGs in the GC. However, the initial Fe/H ratios of Cunha et al.'s sample were likely 0.05-0.1dex lower than reported due to the affore-mentioned self-depletion effect.

From Fig. 3 it is clear that the RSGCs do not follow the radial Galactic Fe/H trend – the clusters exhibit Fe abundances which are $\sim$0.5dex below those of the Cepheids in the inner disk. This plot may simply illustrate the inadequacies of a one-dimensional parameterization of abudance trends, particularly in the inner Galaxy. The presence of physical structures in the inner regions of the disk, such as the Bar, and the ends of the spiral arms, represent large azimuthal fluctuations in stellar/gas density and star-formation rates. As such, it seems unlikely that chemical abundances should be homogeneous around the inner disk. This is a point that we investigate further in Sect. 5.2.3.

5.2.2. *The α-elements: O, Ca, Si, Mg, and Ti*

As with Fe, these elements are again found to be subsolar in relation to H. However, the ratio of α/Fe is solar to within the errors, consistent with a disk population. In Fig. 4 we again put these results in context with measurements of objects at similar $R_{\rm GC}$. In a search of the literature, we have found abundance measurements in the inner disk for O, Mg and Si for Cepheids (Andrievsky et al. 2002), B dwarfs (Smartt et al. 2001; Daflon & Cunha 2004); while we also find O measurements from H II regions (Afflerbach et al. 1997). The H II region measurements are less reliable as they are highly model-dependent – they determine temperatures by matching the amount of ionizing UV flux (inferred from the radio) to model stellar atmospheres, which in itself depends on metallicity. Nevertheless, we include their data for completeness.

Figure 4 again shows that the RSG clusters appear to have systematically lower abundances than other objects located at similar Galacto-centric distances. However, when the B dwarf measurements are included, the discrepancy of the RSGC data appears less striking. Indeed, taken together, the cepheid, RSGC and B dwarf measurements seem to suggest that there be large abundance variations in the inner Galaxy.

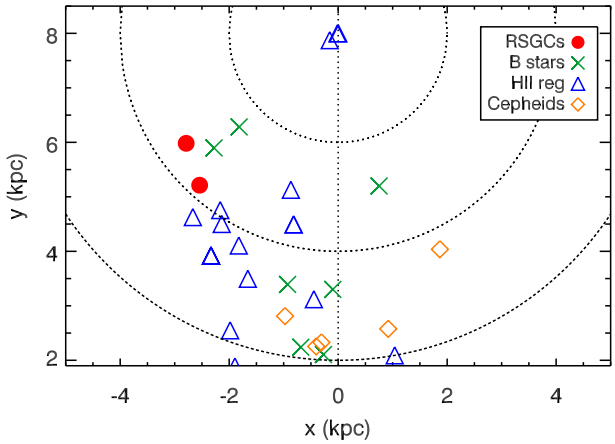

Fig. 5.—: Location in the Galaxy of the B stars, H II regions and Cepheids used as probes of the metallicity gradient. We assume the Galactic centre to be 8 kpc from Earth. The dotted circles show Galacto-centric distances of 2, 4, and 6 kpc. The references for the literature data are given in Table 2

5.2.3. *Azimuthal variations in relative abundances*

As stated in the preceeding sections, the simple one-dimensional parameterization of abundance patterns in a metallicity gradient may be too obtuse when dealing with the inner regions of the Galaxy. Indeed, the presence of the Bar at $R_{\rm GC} \lesssim 4$kpc implies large azimuthal fluctuations in stellar/gas density, hence it is not inconceivable that variations in abundances may also exist.

In Fig. 5, we show the locations of the objects plotted in Figs. 3 and 4 in the X-Y plane. We see that the Cepheids and the RSGCs, which have abundance differences of ∼0.4dex, are separated in physical space by approximately 4 kpc. Curiously, the B dwarfs and H II regions, which have intermediate chemical abundances between the RSGCs and Cepheids, are also located between the two in physical space. This raises the intriguing possibility of large-scale (∼kpc) azimuthal abundance variations in the inner disk.

To explore this prospect further, in Fig. 6 we plot the relative abundances of the Cepheids, B dwarfs, H II regions and RSGCs as a function of their azimuthal angle about the Galactic Centre, $\phi_{\rm GC}$. We choose to plot the abundances as a function of the cosine of the angle, as any periodic variations should show up as linear trends in $\cos(\phi_{\rm GC})$-space. We define the positive direction as being clockwise when viewed from above, and we have rotated the coordinate system such that the RSG clusters, which have the lowest abundances, have $\cos(\phi') = 1$, where $\phi' \equiv \phi_{\rm GC} - \phi_{\rm RSGC}$. In practice this coordinate system transformation made very little difference to the results.

From Fig. 6 we see that, though there is no strong evidence of a gradient in Mg, trends do seem to exist in O and Si. This is true even if the model-dependent H II-region points are removed. We find that the gradients in O and Si, determined from linear regressions, are significant at the $\sim 5\sigma$ level. Further, the gradients are similar in each element to within the uncertainties. When the coordinate system was *not* rotated (see above), this gradient significance was still in excess of 4σ.

These measurements are probing a limited range in azimuth, so these observed gradients are representative of localised fluctuations in abundance levels in the inner disk. Moreover, these fluctuations apparently coincide with the end of the Bar. Given that we find these statistically-significant variations, we identify three statistical explanations for the observed trends which we discuss below.

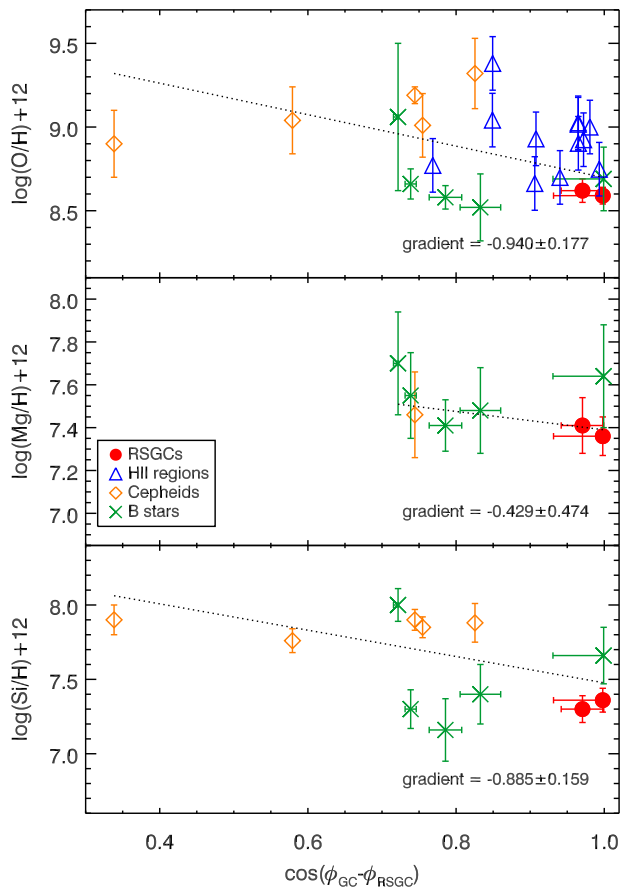

Fig. 6.—: Azimuthal abundance gradients for oxygen, magnesium and silicon, created using objects with Galacto-centric distances of 3.5 to 6.0 kpc. The coordinate system has been rotated such that $(\phi_{\rm GC} - \phi_{\rm RSGC}) \equiv 0^\circ$. The references for the literature data are given in Table 2

Artifacts of random sampling —— If the abundances in the inner Galaxy are uniform, but have large scatter, then a gradient in abundances may be artificially inferred if we happen to sample the extremes of the abundance distribution at the extremes of the observed $\phi_{\rm GC}$ range. This would seem like a plausible explanation for the measured gradient in $\phi_{\rm GC}$, as the data-points in Fig. 6 are few and poorly sampled at the extremes of $\phi_{\rm GC}$.

To investigate quantitatively the likelihood of this scenario, we have performed monte-carlo simulations to generate random abundance levels at the *same* sampling in $\cos(\phi')$-space as the data plotted in Fig. 6. For each simulation, we generated data with uniformly random distribution with a peak-to-peak amplitude of 0.85dex – similar to that of the observed data. We set the uncertainty in each value of $A(X)$ to the same as in the observations at that value of $\cos(\phi')$[3]. We calculated the gradient g and uncertainty σg of the simulated data, and measured the significance of the gradient $Q \equiv g/\sigma g$. The

[3] Setting all measurement uncertainties to ±0.15dex had no effect on the results of our analysis.

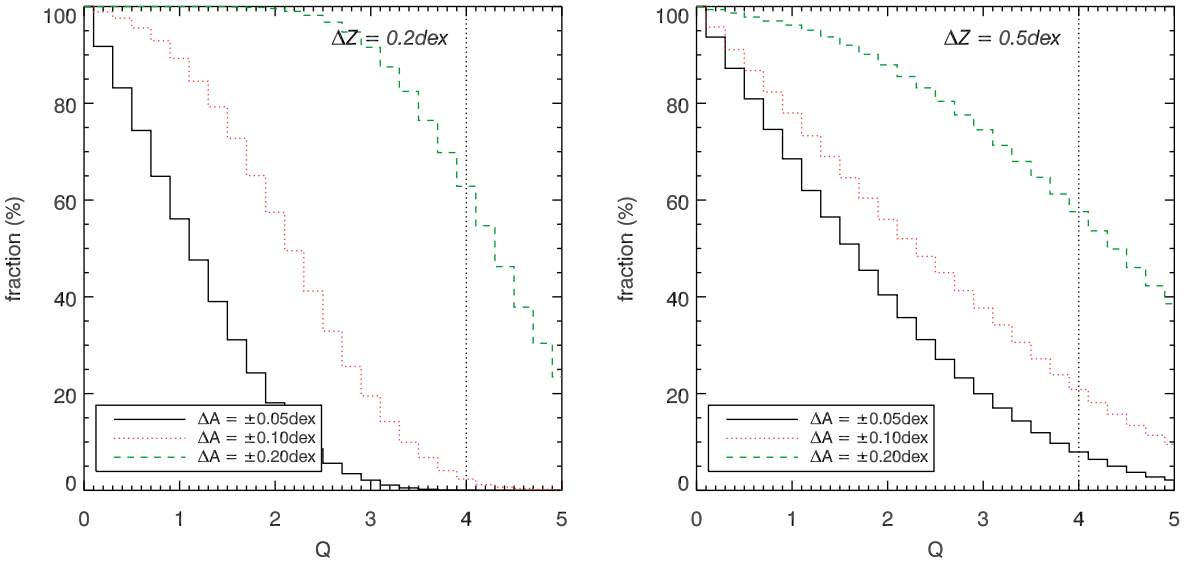

Fig. 7.—: The probability of obtaining a gradient with significance Q ($\equiv g/\sigma g$) for three different values of ΔA, which is defined as systematic difference in the measured abundance of an element when determined from two different methods. We plot simulations for two different *intrinsic* abundance scatters: $\Delta Z = \pm 0.2$dex (left) and $\Delta Z = \pm 0.5$dex (right). The significance of our measured azimuthal gradients in O and Si, $Q = 4$, is indicated by the dotted line. Each plot shows that, for larger systematic differences, the probability of artificially inferring a gradient is higher. Meanwhile, comparison between the two figures shows that gradients are more likely to be inferred if the intrinsic scatter is larger.

simulation was repeated 10^5 times and the frequency of obtaining a measured gradient with significance $Q \geq 4$ was recorded.

We found that the likelihood of measuring a gradient at the $Q = 4$ significance level in the O and Si data was low, ∼14%. As it may be argued that the two RSGC measurements may not be independent of one another, we then repeated the experiment, this time forcing the two RSGC data-points to the same value. This time, the probabilities of obtaining a $Q = 4$ gradient rose to ≈23% for each of O and Si. We repeated this analysis, this time generating random $A(X)$ values from a guassian distribution with standard deviation $\sigma A = 0.3$, the observed spread of the Si abundances. This time, we found that the probability of obtaining $Q = 4$ was 22%, or 30% when the RSGC points were forced to the same value.

From this analysis, we conclude that the measured gradients in Si and O are unlikely to be a result of random sampling. That is to say, if large azimuthal abundance dispersions exist in the inner disk, the likelihood of artificially inferring the gradients we measure from random sampling is $\lesssim$30%.

Systematic offsets between analysis methods –– Another explanation for the observed gradient may be that the abundances in the inner disk are uniform, but a systematic offset exists between abundances measured using different methods. For example, Si abundances measured from Cepheids may yield values which are systematically higher than those measured from RSGs, even though the *true* abundances of the two objects are the same. Indeed, one may argue from the bottom panel of Fig. 6 that the Si abundances of the Cepheids are constant to within the errors, as are the two RSG clusters, with the two classes of objects offset from one another by ∼0.5dex.

We performed a quantitative investigation of this, again using monte-carlo simulations. We assumed that the abundances Z in the inner disk are uniform, with an intrinsic peak-to-peak scatter of ΔZ. We randomly generated abundance values at the same distribution in $\cos(\phi')$ as the data in Fig. 6. We then artificially raised the abundances of the cepheid points by ΔA, and decreased the RSGC points by the same quantity. That is, a value of $\Delta A = \pm 0.2$ separates the two classes of object by 0.4dex in abundance space. We again forced the RSGC abundaces to be the same, as these measurements may not be independent of one another. The abundances of the B stars were randomized, with a distribution of ±0.4dex about the mean value, similar to the data in Fig. 6. At the end of each simulation, the gradient g and its significance Q was measured, and the experiment repeated 10^5 times.

In Fig. 7, we plot the likelihood of measuring a statistically significant gradient for three different values of ΔA, using the same $\cos(\phi')$ values as those in the bottom panel of Fig. 6. We then reproduce this analysis for two different *intrinsic* abundance scatters, ΔZ. For example, the right-hand panel of Fig. 7 shows the fraction of simulations for which a gradient with significance Q is measured for data with a peak-to-peak abundance scatter of ΔZ =0.5dex. In this panel, for a systematic offset $\Delta A = \pm 0.1$dex – the same as quoted uncertainties in the data – the probability of inferring a $Q > 4$ gradient is 20%. For an offset of $\Delta A = \pm 0.2$, which is the value typically quoted as being the absolute uncertainty on any abundance measurement, the probability is raised to 50-60%.

From this analysis, we conclude that it is possible that the azimuthal abundance gradient we measure is due to systematic offsets between differing measurement techniques. However, for a 50% probability of obtaining

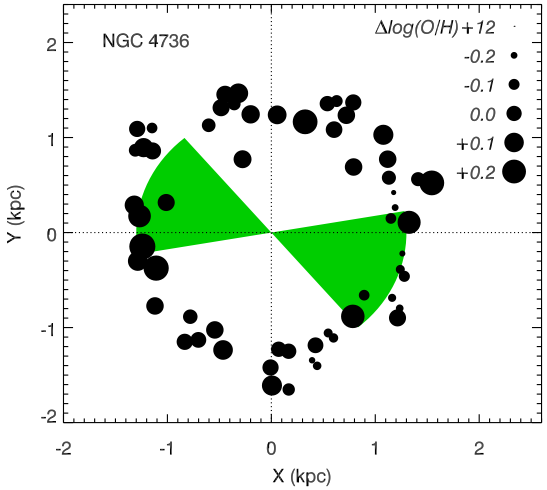

Fig. 8.—: Azimuthal [O/H] variations in NGC 4736. Symbol sizes represent the magnitude of the abundance levels in the various H IIregions that surround the central region, as indicated by the legend. The shaded region denotes the rough extent and position angle (110±30°) of the galaxy's bar.

the $Q = 4$ gradients we observe, the offset between the RSGCs and the Cepheids must be large, ∼0.4dex (i.e. $\Delta A = \pm 0.2$). We note that in the Galactic Centre, we found good agreement (better than ±0.2dex) between our analysis of RSGs and that of other classes of objects such as Luminous Blue Variables (Najarro et al. 2008; Davies et al. 2008b).

Real trends –– Having studied two scenarios that could lead us to artificially measure a gradient where none existed, we now discuss the possibility that the measured azimuthal abundance variations are real. If such behaviour exists in our Galaxy, then it is reasonable to assume that it should also be present in external galaxies. In the following section, we investigate the presence of azimuthal abundance variations in the face-on spiral NGC 4736.

5.2.4. *Case-study: NGC 4736 (≡ M94)*

In looking for an azimuthal abundance gradient in an external galaxy, we have chosen this object for several reasons. Firstly, while not having the exact same type as our own Galaxy, it is a spiral with a central bar, and is relatively face-on (Block et al. 1994). Secondly, it has a ring of H II regions in the inner disk, which are well sampled in azimuth (Lynds 1974). Thirdly, oxygen abundances of these H II regions are present in the literature: Martin & Belley (1997) studied the H II region ring with narrow-band filters to measure the fluxes of certain diagnostic lines in the optical, and used them to derive abundances. However, the authors did not use the abundances to study azimuthal variations, only the presence of a radial gradient. This study utilized a homogeneous methodology, and so we do not have to take into account systematic errors induced by differing analysis techniques.

In Fig. 8 (*left*) we plot the locations of the H II regions in the $X - Y$ plane, corrected for the galaxy's inclination. The size of the plotting symbols indicates the magnitude of the abundance of each H II region with respect

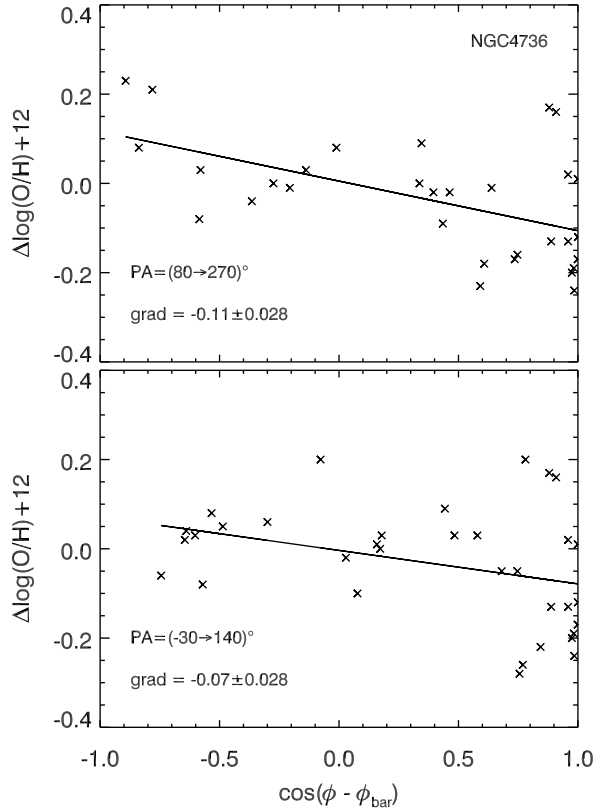

Fig. 9.—: The abundance ratio [O/H] as a function of azimuthal angle, with the coordinate system rotated such that the central bar ($\phi_{/rmbar}$=110±30°) is oriented at $\cos(\phi') = 1$. In the top panel, we plot [O/H] versus azimuthal angle in the clockwise direction away from the bar, plotting those points with $\phi > 80°(=\phi_{\rm bar} - \sigma\phi_{\rm bar})$. Similarly, in the bottom panel we [O/H] as a function of $\cos(\phi)$ in the anti-clockwise direction, plotting those points with $\phi < 140°(= (\phi_{\rm bar} + \sigma\phi_{\rm bar})$

to the global average. To the eye, it seems that the abundances in the lower-right quadrant of the figure tend to be lower than average; while at the left edge of the ring at $(X, Y) \approx (-1, 0)$ the abundances are highest. Interestingly, the minimum in abundance levels corresponds roughly with the end of the bar ($\phi_{\rm bar} = 110\pm30°$, indicated by the shaded region in Fig. 8 – Block et al. 1994; Wong & Blitz 2000). This is similar to the trend seen in our own Galaxy, where the abundance minimum is found in the RSG clusters located at the end of the Galaxy's Bar.

In Fig. 9, we plot the abundance levels as a function of the cosine of the azimuthal angle. Again, as in Fig. 6 we have rotated the coordinate system to such that the minimum abundances correspond to $\cos(\phi) = 1.0$. For this rotation angle we adopt the position angle of the bar, 110±30°. The top panel of Fig. 9 shows the abundance trend as a function of $\cos(\phi)$ in the clockwise direction from the lower limit of the bar's orientation (110°- 30°= 80°). Similarly, in the bottom panel we show the abundance trend in the anti-clockwise direction up to the upper limit of the bar's orientation (140°). We opt to plot the abundance variations in the two directions separately, as the trends in each direction are not necessarily similar.

In each panel of Fig. 9 we make a linear fit to the [O/H] distribution and indicate on the plot the measured gra-

dient and its uncertainty. The maximum position angle that we have chosen to plot in each panel, $\phi_{bar}\pm160°$, was somewhat arbitrarily chosen to illustrate a wide range of azimuth as well as include a sufficiently large number of data-points, though we note that the range chosen does not significantly affect Q-values of the measured gradients.

From the two panels of Fig. 9 we see that abundance gradients are measured at the $Q = 4$ (clockwise) and $Q = 2$ (anti-clockwise) levels. Though tentative, this does provide some support for the idea of localised azimuthal abundance variations in the inner disk of NGC 4736. We again state that, as in our analysis of the inner Galaxy, these 'gradients' are more likely to be indicative of systematic undulations in abundance levels rather than true sinusoidal variations with azimuthal angle.

5.2.5. *Bars, and azimuthal abundance variations*

To summarize the results of the previous section, we find it unlikely that the azimuthal abundance patterns we observe in the inner Galaxy are an artifact of random sampling. We cannot rule out that the observed variations result from systematic offsets between different methodologies. However, in using data from a homogeneous study of the external galaxy NGC 4736 where we are able to make a differential analysis, we find tentative evidence for similar abundance variations. In each case, the lowest abundances were observed at the end of the central bar.

Given these apparent azimuthal variations in abundances seen in both our Galaxy and NGC 4736, we now discuss how such could patterns arise. It is known that there is a link between abundance trends and the presence of bars – radial abundance gradients tend to be flatter in barred spirals than in unbarred spirals (Zaritsky et al. 1994; Martin & Roy 1994). Indeed, the observed abundance gradient in our Galaxy is typical of barred spirals, and much shallower than unbarred spirals. The common explanation for this is that radial gas motions induced by the bar potential smooth-out any pre-existing abundance gradient on timescales of a few $\times$100Myr. However, this can introduce significant azimuthal variations, especially between the spiral arms and the inter-arm regions, due to intense but patchy star-formation (Friedli et al. 1994; Friedli & Benz 1995).

In NGC 4736, kinematic studies have shown that the H II ring is coincident with the outer Lindblad resonance of the bar and the inner Lindblad resonance of the central bulge. The ring itself is likely a result of radial inward gas motions outside of this resonance zone and outward motions inside (Wong & Blitz 2000; Muñoz-Tuñón et al. 2004). The ensuing star-formation within the ring, as the colliding material is shocked, has been shown to be patchy from CO and Hα observations (Wong & Blitz 2000). As the timescale for chemical enrichment by massive stars is comparable to the dynamical timescales in the region of the bar (few $\times$100Myr), it is conceivable that notable fluctuations in the azimuthal abundances of the α-elements would survive. Similarly, in our Galaxy, azimuthal abundance variations could be produced by intense but patchy star-formation in the region of the Bar's outer Lindblad resonance at $R_{\rm GC}\approx4$ kpc. Indeed, this starburst episode could be responsible for creating the RSG clusters. However, it is unclear how this effect would show itself in the Fe abundances, as the enrichment timescale for this element is longer ($\sim 10^8 - 10^9$yr). Clearly, the abundances in the inner Galactic disk require further study, and would benefit from a homogenous study such as that of NGC 4736 by Martin & Belley (1997). Massive young clusters such as RSGC1 and RSGC2, from which abundances of several elements may be determined in the near-IR, may represent the best tool with which to do this. Though known examples of such clusters are currently low in number, searches of infrared Galactic plane surveys have revealed many more candidates, and the number of known young massive clusters in the inner Galaxy looks set to rise in the next few years.

6. CONCLUSIONS

We have used high-resolution near-infrared spectroscopy and detailed spectral synthesis to determine the chemical abundances of the two Scutum Red Supergiant clusters, RSGC1 and RSGC2, which are located in the inner Galaxy close to the end of the Bar. Our results can be summarized as follows:

- The stars atmopsheres are carbon-depleted, and the average levels of depletion agree well with the predictions of rotating single-star models. Non-rotating models predict C/Fe surface abundances which are higher than observed.

- The average iron abundances (Fe/H) are found to be sub-solar by 0.2-0.3dex. This is in apparent conflict with the Fe abundances of objects at similar Galactocentric distances, which have typically been found to be $\sim$0.5dex higher.

- The abundances of the α-elements are also sub-solar. The ratio of α/Fe is fully consistent with solar, as is typical for objects in the thin disk.

To explain the apparently unusual abundances of the RSG clusters with respect to other objects in the inner disk, we have collected several abundance measurements of different classes of object in the literature. It appears that large azimuthal abundance variations exist in the inner disk, as is predicted by theory for the secular evolution of galaxies with bars. Further, we find that the objects in the inner disk with strongly super-solar abundances are typically located at negative Galactic longitude l, while the RSG clusters are located at positive l. We find tentative evidence for large-scale azimuthal abundance variations in the data, significant at the 4-5σ-level. The presence of these variations can only be explained away if abundance studies of different types of object have significant systematic offsets from one another. In a differential analysis study of the external barred galaxy NGC 4736 using homogeneous methodology, we again find tentative evidence for large-scale azimuthal abundance fluctuations. We suggest that these results for both our Galaxy and NGC 4736 are consistent with the predictions of the Friedi & Benz model for chemical evolution in barred spirals, whereby the bar potential which causes a pile-up of material at the outer Lindblad resonance results in intense but patchy star-formation in the inner region of the disk. As the dynamical timescale

is comparable to the timescale for chemical enrichment, large azimuthal abundance variations can form.

Acknowledgements: For many useful discussions, we would like to thank Nate Bastian, Bob Benjamin, Paul Crowther, Katia Cunha, John Eldridge, Maria Messineo, and Rob Kennicutt. We thank Bengt Gustafsson for providing us with his group's molecular line-list for CN. We also thank the anonymous referee for several comments and suggestions which helped us improve the paper. The material in this work is supported by NASA under award NNG 05-GC37G, through the Long-Term Space Astrophysics program. This research was performed in the Rochester Imaging Detector Laboratory with support from a NYSTAR Faculty Development Program grant. The data presented here were obtained at the W. M. Keck Observatory, which is operated as a scientific partnership among the California Institute of Technology, the University of California, and the National Aeronautics and Space Administration. The Observatory was made possible by the generous financial support of the W. M. Keck Foundation. This research has made use of IDL software packages, and the GSFC IDL library.

REFERENCES

Afflerbach, A., Churchwell, E., & Werner, M. W. 1997, ApJ, 478, 190
Andrievsky, S. M., Bersier, D., Kovtyukh, V. V., Luck, R. E., Maciel, W. J., Lépine, J. R. D., & Beletsky, Y. V. 2002, A&A, 384, 140
Asplund, M., Grevesse, N., & Sauval, A. J. 2005, in Astronomical Society of the Pacific Conference Series, Vol. 336, Cosmic Abundances as Records of Stellar Evolution and Nucleosynthesis, ed. T. G. Barnes, III & F. N. Bash, 25–+
Ballero, S. K., Matteucci, F., Origlia, L., & Rich, R. M. 2007, A&A, 467, 123
Benjamin, R. A., Churchwell, E., Babler, B. L., Indebetouw, R., Meade, M. R., Whitney, B. A., Watson, C., Wolfire, M. G., Wolff, M. J., Ignace, R., Bania, T. M., Bracker, S., Clemens, D. P., Chomiuk, L., Cohen, M., Dickey, J. M., Jackson, J. M., Kobulnicky, H. A., Mercer, E. P., Mathis, J. S., Stolovy, S. R., & Uzpen, B. 2005, ApJ, 630, L149
Bensby, T., Feltzing, S., & Lundström, I. 2004, A&A, 415, 155
Biemont, E. & Grevesse, N. 1973, Atomic Data and Nuclear Data Tables, 12, 217
Block, D. L., Bertin, G., Stockton, A., Grosbol, P., Moorwood, A. F. M., & Peletier, R. F. 1994, A&A, 288, 365
Clark, J. S., Muno, M. P., Negueruela, I., Dougherty, S. M., Crowther, P. A., Goodwin, S. P., & de Grijs, R. 2008, A&A, 477, 147
Cunha, K., Sellgren, K., Smith, V. V., Ramirez, S. V., Blum, R. D., & Terndrup, D. M. 2007, ApJ, 669, 1011
Cunha, K. & Smith, V. V. 2006, ApJ, 651, 491
Daflon, S. & Cunha, K. 2004, ApJ, 617, 1115
Davies, B., Figer, D. F., Kudritzki, R.-P., MacKenty, J., Najarro, F., & Herrero, A. 2007, ApJ, 671, 781
Davies, B., Figer, D. F., Law, C. J., Kudritzki, R.-P., Najarro, F., Herrero, A., & MacKenty, J. W. 2008a, ApJ, 676, 1016
Davies, B., Origlia, L., Kudritzki, R.-P., Figer, D. F., Rich, R. M., & Najarro, F. 2008b, ArXiv e-prints
Eldridge, J. J., Izzard, R. G., & Tout, C. A. 2008, MNRAS, 384, 1109
Figer, D. F., Gilmore, D., Kim, S. S., Morris, M., Becklin, E. E., McLean, I. S., Gilbert, A. M., Graham, J. R., Larkin, J. E., Levenson, N. A., & Teplitz, H. I. 2003, ApJ, 599, 1139
Figer, D. F., MacKenty, J. W., Robberto, M., Smith, K., Najarro, F., Kudritzki, R. P., & Herrero, A. 2006, ApJ, 643, 1166
Friedli, D. & Benz, W. 1995, A&A, 301, 649
Friedli, D., Benz, W., & Kennicutt, R. 1994, ApJ, 430, L105
Fulbright, J. P., McWilliam, A., & Rich, R. M. 2006, ApJ, 636, 821
—. 2007, ApJ, 661, 1152
Gotthelf, E. V. & Halpern, J. P. 2008, ApJ, 681, 515
Grevesse, N. & Sauval, A. J. 1998, Space Science Reviews, 85, 161
Huber, K. P. & Herzberg, G. 1979, Molecular Spectra and Molecular Structure Constants of Diatomic Molecules (New York: Van Nostrand)
Johnson, H. R., Bernat, A. P., & Krupp, B. M. 1980, ApJS, 42, 501
Larsen, S. S., Origlia, L., Brodie, J., & Gallagher, J. S. 2008, MNRAS, 383, 263
Lecureur, A., Hill, V., Zoccali, M., Barbuy, B., Gómez, A., Minniti, D., Ortolani, S., & Renzini, A. 2007, A&A, 465, 799
López-Corredoira, M., Garzón, F., Beckman, J. E., Mahoney, T. J., Hammersley, P. L., & Calbet, X. 1999, AJ, 118, 381
Luck, R. E., Kovtyukh, V. V., & Andrievsky, S. M. 2006, AJ, 132, 902
Lynds, B. T. 1974, ApJS, 28, 391
Maciel, W. J. & Quireza, C. 1999, A&A, 345, 629
Maeder, A. & Meynet, G. 2001, A&A, 373, 555
Martin, P. & Belley, J. 1997, A&A, 321, 363
Martin, P. & Roy, J.-R. 1994, ApJ, 424, 599
McLean, I. S., Becklin, E. E., Figer, D. F., Larson, S., Liu, T., & Graham, J. 1995, in Presented at the Society of Photo-Optical Instrumentation Engineers (SPIE) Conference, Vol. 2475, Proc. SPIE Vol. 2475, p. 350-358, Infrared Detectors and Instrumentation for Astronomy, Albert M. Fowler; Ed., ed. A. M. Fowler, 350–358
Meléndez, J., Asplund, M., Alves-Brito, A., Cunha, K., Barbuy, B., Bessell, M. S., Chiappini, C., Freeman, K. C., Ramírez, I., Smith, V. V., & Yong, D. 2008, A&A, 484, L21
Meléndez, J. & Barbuy, B. 1999, ApJS, 124, 527
Mengel, S., Lehnert, M. D., Thatte, N. A., Vacca, W. D., Whitmore, B., & Chandar, R. 2008, ArXiv e-prints, 805
Meynet, G. & Maeder, A. 2000, A&A, 361, 101
Muñoz-Tuñón, C., Caon, N., & Aguerri, J. A. L. 2004, AJ, 127, 58
Najarro, F., Figer, D. F., Hillier, D. J., Geballe, T. R., & Kudritzki, R.-P. 2008, ApJ, in press
Origlia, L., Ferraro, F. R., Bellazzini, M., & Pancino, E. 2003, ApJ, 591, 916
Origlia, L., Moorwood, A. F. M., & Oliva, E. 1993, A&A, 280, 536
Origlia, L., Rich, R. M., & Castro, S. 2002, AJ, 123, 1559
Rich, R. M. & Origlia, L. 2005, ApJ, 634, 1293
Rolleston, W. R. J., Smartt, S. J., Dufton, P. L., & Ryans, R. S. I. 2000, A&A, 363, 537
Schaerer, D., Charbonnel, C., Meynet, G., Maeder, A., & Schaller, G. 1993, A&AS, 102, 339
Schaller, G., Schaerer, D., Meynet, G., & Maeder, A. 1992, A&AS, 96, 269
Smartt, S. J., Venn, K. A., Dufton, P. L., Lennon, D. J., Rolleston, W. R. J., & Keenan, F. P. 2001, A&A, 367, 86
Sneden, C. & Lambert, D. L. 1982, ApJ, 259, 381
Wong, T. & Blitz, L. 2000, ApJ, 540, 771
Yong, D., Carney, B. W., Teixera de Almeida, M. L., & Pohl, B. L. 2006, AJ, 131, 2256
Zaritsky, D., Kennicutt, Jr., R. C., & Huchra, J. P. 1994, ApJ, 420, 87

APPENDIX

Appendix: The chemical abundances of the stars observed in each cluster. Star identification numbers are taken from Figer et al. (2006) and Davies et al. (2007)

TABLE 3:
Elemental abundances for each star studied. Abundances for each element X are expressed in the form $A(X) = \log(X/\mathrm{H}) + 12$. For reference, the solar abundances derived by Asplund et al. (2005) are also shown.

Star	T_{eff}	A(Fe)	A(O)	A(Si)	A(Mg)	A(Ca)	A(Ti)	A(C)
Solar Abundances (Asplund et al. 2005)								
–	–	7.45	8.66	7.51	7.53	6.31	4.90	8.39
–	–	± 0.05	± 0.05	± 0.04	± 0.09	± 0.04	± 0.06	± 0.05
RSGC1 Abundances								
1	3600	7.36	8.58	7.21	7.57	6.16	4.98	7.82
–	–	± 0.09	± 0.08	± 0.14	± 0.12	± 0.07	± 0.10	± 0.09
2	3600	7.30	8.59	7.25	7.28	6.19	4.72	7.92
–	–	± 0.08	± 0.09	± 0.14	± 0.12	± 0.07	± 0.10	± 0.09
3	3400	7.40	8.58	7.30	7.48	6.24	5.02	7.92
–	–	± 0.09	± 0.13	± 0.15	± 0.13	± 0.08	± 0.12	± 0.09
4	3800	7.35	8.76	7.32	7.36	6.28	5.02	7.92
–	–	± 0.09	± 0.07	± 0.11	± 0.12	± 0.07	± 0.08	± 0.09
5	3600	7.29	8.63	7.22	7.28	6.20	4.92	7.97
–	–	± 0.08	± 0.10	± 0.14	± 0.12	± 0.07	± 0.10	± 0.09
6	3400	7.41	8.58	7.35	7.64	6.29	5.02	8.02
–	–	± 0.08	± 0.12	± 0.15	± 0.13	± 0.08	± 0.12	± 0.09
7	3600	7.27	8.54	7.25	7.28	6.12	4.82	7.92
–	–	± 0.08	± 0.09	± 0.14	± 0.12	± 0.07	± 0.09	± 0.09
8	3600	7.32	8.61	7.25	7.27	6.18	4.92	8.02
–	–	± 0.08	± 0.09	± 0.14	± 0.12	± 0.07	± 0.10	± 0.09
9	3400	7.37	8.53	7.25	7.54	6.19	4.92	7.92
–	–	± 0.09	± 0.11	± 0.15	± 0.13	± 0.08	± 0.10	± 0.09
10	3600	7.31	8.72	7.35	7.48	6.22	5.02	8.02
–	–	± 0.09	± 0.10	± 0.14	± 0.12	± 0.08	± 0.11	± 0.09
11	3600	7.29	8.57	7.35	7.38	6.21	4.92	8.02
–	–	± 0.08	± 0.10	± 0.14	± 0.12	± 0.07	± 0.10	± 0.09
12	3800	7.38	8.70	7.53	7.53	6.26	4.92	8.02
–	–	± 0.09	± 0.07	± 0.11	± 0.12	± 0.06	± 0.07	± 0.09
13	3800	7.27	8.68	7.25	7.28	6.18	4.72	7.82
–	–	± 0.07	± 0.07	± 0.11	± 0.12	± 0.07	± 0.08	± 0.09
14	3600	7.25	8.54	7.35	7.38	6.13	4.92	7.92
–	–	± 0.08	± 0.10	± 0.14	± 0.12	± 0.07	± 0.10	± 0.09
RSGC2 Abundances								
2	3600	7.04	8.37	7.05	7.08	6.01	4.73	7.72
–	–	± 0.08	± 0.09	± 0.13	± 0.12	± 0.06	± 0.08	± 0.09
3	3600	7.22	8.60	7.24	7.28	6.11	4.92	7.92
–	–	± 0.08	± 0.10	± 0.14	± 0.12	± 0.07	± 0.10	± 0.09
5	3600	7.29	8.54	7.25	7.25	6.18	4.92	7.92
–	–	± 0.08	± 0.10	± 0.14	± 0.12	± 0.07	± 0.10	± 0.09
6	3600	7.30	8.60	7.50	7.53	6.21	4.92	7.82
–	–	± 0.08	± 0.10	± 0.14	± 0.12	± 0.07	± 0.10	± 0.09
8	3600	7.30	8.70	7.45	7.38	6.23	4.92	8.02
–	–	± 0.08	± 0.08	± 0.13	± 0.12	± 0.08	± 0.11	± 0.09
9	3600	7.30	8.58	7.35	7.38	6.21	4.92	7.92
–	–	± 0.08	± 0.10	± 0.14	± 0.12	± 0.07	± 0.10	± 0.09
10	3600	7.27	8.54	7.35	7.22	6.15	4.92	7.92
–	–	± 0.08	± 0.10	± 0.14	± 0.12	± 0.07	± 0.10	± 0.09
11	3600	7.26	8.64	7.35	7.31	6.21	4.92	7.92
–	–	± 0.08	± 0.10	± 0.14	± 0.12	± 0.07	± 0.10	± 0.09
14	3600	7.29	8.62	7.35	7.38	6.21	4.92	7.82
–	–	± 0.08	± 0.09	± 0.14	± 0.12	± 0.07	± 0.10	± 0.09
15	3600	7.26	8.56	7.35	7.38	6.16	4.92	7.82
–	–	± 0.08	± 0.10	± 0.14	± 0.12	± 0.07	± 0.10	± 0.09
21	3600	7.32	8.54	7.35	7.38	6.13	4.92	7.82
–	–	± 0.08	± 0.10	± 0.14	± 0.12	± 0.07	± 0.10	± 0.09
29	3800	7.29	8.59	7.45	7.49	6.20	4.92	7.92
–	–	± 0.08	± 0.08	± 0.11	± 0.12	± 0.07	± 0.08	± 0.09